An Optimized Compact Rat Race at 2.45 GHz

Stefano Maddio, Giuseppe Pelosi, Monica Righini, and Stefano Selleri[*]

Abstract—A compact microstrip rat race attained by artificially shortening its lines by inserting stubs is presented. The design starts with a preliminary theoretical length reduction where quarter wavelength lines are shortened thanks to shunt open circuit stubs placed in the line mid-points. Such a preliminary design is then optimized via particle swarm optimization (PSO) within a full wave electromagnetic CAD, also bending the stubs to attain maximum compactness. The resulting design occupies an area up to only 37% of a conventional rat race, with performances comparable to those of a standard rat race.

1. INTRODUCTION

Rat races, or ring hybrids, are microstrip devices commonly used at microwave frequencies [1–3], and yet, because they rely on a ring whose circumference is 1.5λ, they occupy an area on the printed board about $0.2\lambda^2$, with λ being the wavelength in the microstrip.

This dimensional drawback is shared with other hybrid junctions, like branch coupler [2, 4]. To the latter the authors have applied a miniaturization technique based on the length reduction (or augmentation, if needed) of the quarter wavelength sections by introducing stubs at line ends [5–7].

In this contribution, a similar technique is applied to the rat race. In [6, 8], stubs were applied at line ends, and some lines were shortened while others were lengthened so as to have the stubs mutually cancel out almost completely.

In this paper, all lines need to be shortened, and stubs are better placed at line midpoints to attain a higher device symmetry. This is a design choice similar to the one in [9] and [10].

Such a desired shortening of the quarter wavelength lines can be attained theoretically as described in following Section 2, and yet, while stubs can be easily accommodated outside the rat race circle, this would not lead to a compact layout. Stubs are to be placed inside the circle as shown in Section 3. This implies not only higher coupling but also the need to bend the stubs, implying even more complex couplings and design.

The relevance of coupling phenomena is such that even semi-empirical models like [11] introduced in commercial circuit simulator do not suffice to take into account them, hence a full wave simulator is needed, and to tune the theoretical design, an optimization procedure based on the particle swarm paradigm [12] is applied to the full wave simulation.

It is worth mentioning that in [13] a very compact solution for the rat race was obtained, but at a relatively low frequency (under 1 GHz) and at the price of narrow bandwidth of operation. Other compact solutions are detailed later on in a comparative table.

Two of the optimized designs attained are realized and characterized. Results, both simulated and measured, are shown in Section 4. The two designs show, respectively, an area of $0.10\lambda^2$ and $0.07\lambda^2$ hence about half that of a standard rat race in the first, and about one third in the second.
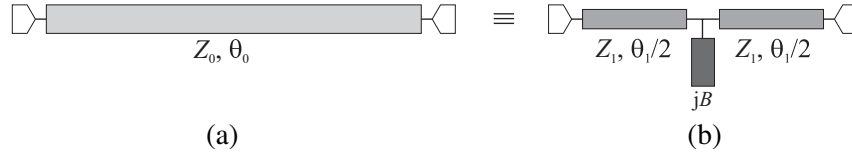
2. CENTRALLY LOADED SHORTENED DELAY LINE

Figure 1 shows the basic idea behind the shortening of a delay line by resorting to a centrally placed shunt reactive load, which in turn is realized via a stub. Such an equivalence of course is exact only at the design frequency f_0.

(a)   (b)

Figure 1. (a) Delay line of electrical length θ_0 and characteristic impedance Z_0. (b) Equivalent delay line of different electric length θ_1 — either shorter or longer than θ_0 — and characteristic impedance Z_1, with a central reactive load of susceptance jB.

In a chain matrix C representation, the delay line on the left in Figure 1 is that of a line of electrical length θ_0 and characteristic impedance Z_0:

$$C_0 = \begin{bmatrix} \cos\theta_0 & jZ_0 \sin\theta_0 \\ j\dfrac{1}{Z_0}\sin\theta_0 & \cos\theta_0 \end{bmatrix} \tag{1}$$

While the device on the right in Figure 1 is characterized by the cascade of two delay lines of electric length $\theta_1/2$ and characteristic impedance Z_1 and a concentrated shunt load, centrally placed, respectively:

$$C_1 = \begin{bmatrix} \cos\left(\theta_1/2\right) & jZ_1 \sin\left(\theta_1/2\right) \\ j\dfrac{1}{Z_1}\sin\left(\theta_1/2\right) & \cos\left(\theta_1/2\right) \end{bmatrix} \tag{2}$$

$$C_2 = \begin{bmatrix} 1 & 0 \\ jB & 1 \end{bmatrix} \tag{3}$$

The complete device chain matrix is given by $C_d = C_1 C_2 C_1$ and is:

$$C_d = \begin{bmatrix} \cos\theta_1 - \dfrac{1}{2}BZ_1\sin\theta_1 & jZ_1\sin\left(\theta_1/2\right)\left[\cos\left(\theta_1/2\right) - BZ_1\sin\left(\theta_1/2\right)\right] \\ j\dfrac{1}{Z_1}\cos\left(\theta_1/2\right)\left[\sin\left(\theta_1/2\right) + BZ_1\cos\left(\theta_1/2\right)\right] & \cos\theta_1 - \dfrac{1}{2}BZ_1\sin\theta_1 \end{bmatrix} \tag{4}$$

It is possible to enforce $C_0 = C_d$, and having chosen the device electrical length θ_1 as a degree of freedom, the result is:

$$\begin{cases} Z_1 = Z_0 \cos\left(\theta_1/2\right) \dfrac{1 - \cos\theta_0}{\sin\left(\theta_1/2\right)\sin\theta_0} \\[4mm] B = \dfrac{1}{Z_0}\dfrac{\sin\theta_0}{\cos^2\left(\theta_1/2\right)}\dfrac{\cos\theta_1 - \cos\theta_0}{1 - \cos\theta_0} \end{cases} \tag{5}$$

The device is hence an *equivalent delay line*.

By analyzing these equations as a function of the original, standard, delay line length θ_0 and of the desired equivalent delay line length θ_1, the graphs in Figures 2 and 3, showing normalized impedance Z_1/Z_0 and susceptance BZ_0 required, are obtained. This of course, being given in terms of the electrical length of the lines, is an equivalence which holds only at the design frequency f_0. This is even more true if, in a microstrip realization, the susceptance jB is realized via an open-ended stub.

For completeness, Figures 4 and 5 show the behavior of such a device, implemented with ideal transmission lines and open-ended stubs, for a delay line of $\lambda/4$ ($\theta_0 = \pi/2$) at 3 GHz and for three shorter equivalent delay lines, respectively $\lambda/6$, $\lambda/8$, and $\lambda/16$ long.

The limits in band of the equivalent delay line is apparent, and bandwidth narrows as the equivalent delay line is made shorter, but this is not an issue in the present application, with the rat race being inherently narrow-banded, since its functioning relies on lines a quarter wavelength long.
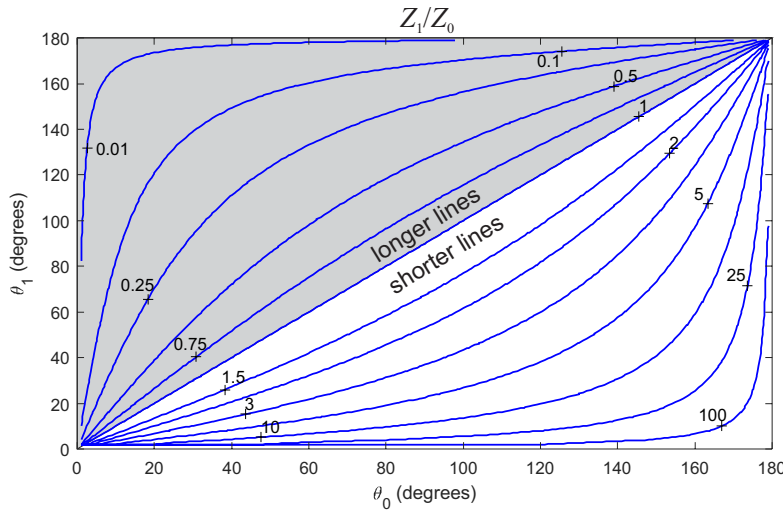
Figure 2. Normalized impedance Z_1/Z_0 as a function of delay line length θ_0 and desired equivalent delay line length θ_1.
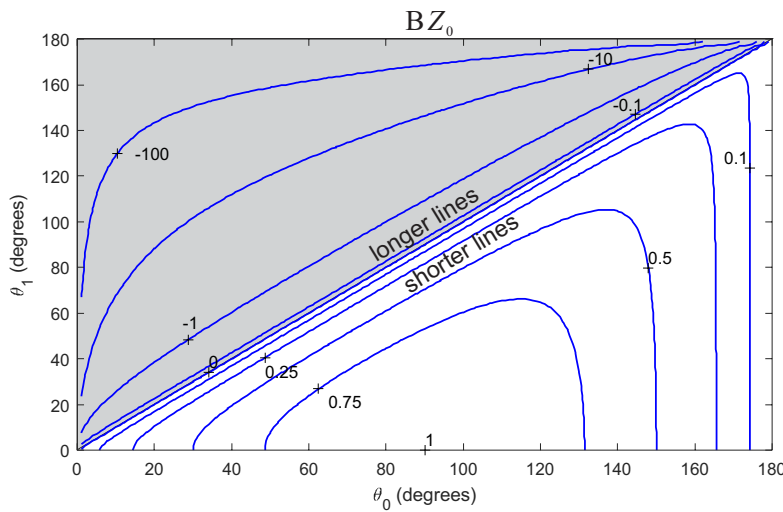
Figure 3. Normalized susceptance BZ_0 as a function of delay line length θ_0 and desired equivalent delay line length θ_1.

3. COMPACT RAT RACE LAYOUT AND OPTIMIZATION

Figure 6 shows the general layout of the compact rat race proposed. The three quarter wavelength ring arcs are reduced via a center stub, as described in the previous section. The $3/4\lambda$ arc is not shortened with a single stub, but rather considered as a cascade of three quarter wavelength arcs, each of which is then shortened. This enforces a higher symmetry, with six identical stubs on the circumference intercalated with the ports.

To minimize the number of optimization variables, the geometrical parameters in Table 1 are defined. The width of the feeding microstrip, W, has been fixed and chosen to have $50\,\Omega$ ports.

The nominal values of R_{in}, W_r, W_s, and overall length of the stub are derived from the theory outlined in the previous section and are considered as central values within an appropriate variation range within the PSO optimization procedure.

First optimizations used all of the parameters in Table 1. With a cost function requiring at least $-25\,\mathrm{dB}$ of matching at ports ($[S_{11}, S_{22}, S_{33}, S_{44}] < -25\,\mathrm{dB}$) and the same value for isolation
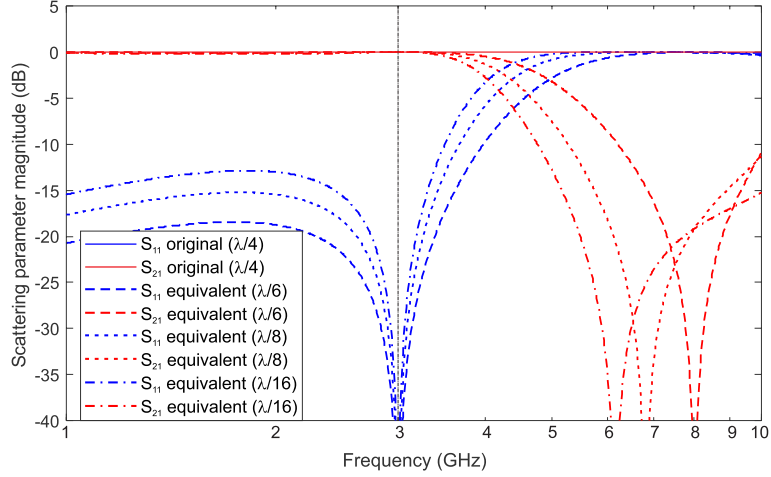
Figure 4. Amplitudes of the scattering parameters of a standard delay line $\lambda/4$ long and of three, shorter, equivalent delay lines.
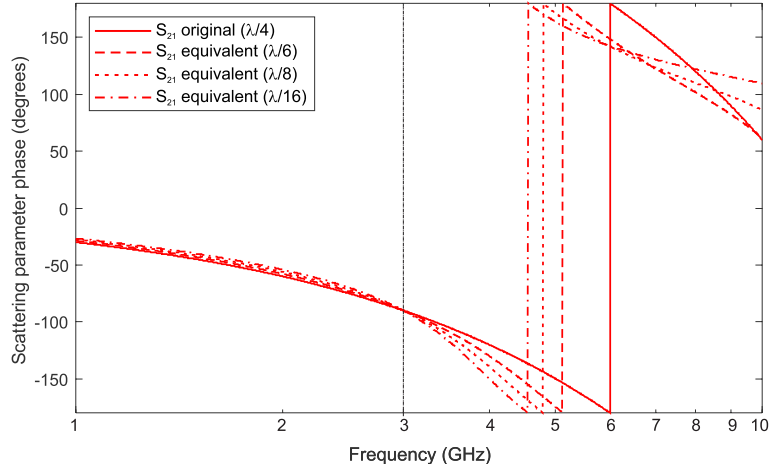

Figure 5. Phase of the transmission parameter of a standard delay line $\lambda/4$ long and of three, shorter, equivalent delay lines.

Table 1. Geometrical parameters for the layout.

| Parameter	Description
R_{in}	internal radius of the microstrip ring
W_r	width of the microstrip ring
W_s	width of the stub
l_1	length of the stub first section
α	angular amplitude of the stub second section
l_2	length of the stub third section
c_1 and c_2	chamfers for better electromagnetic bend behavior

($[S_{31}, S_{42}] < -25\,\text{dB}$) and the remaining parameters at half power ($S_{21}, S_{41}, S_{32}, S_{4,3} = -3\,\text{dB}$), the S matrix of course being symmetrical.
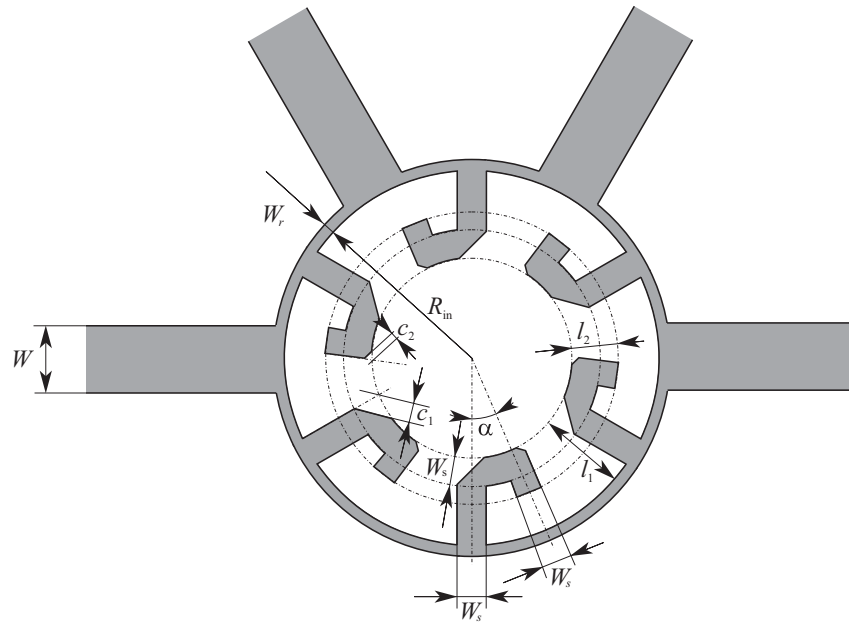
Figure 6. Geometry of the compact rat race, with bent internal stubs and quotes.

Optimization was carried out using particle swarm optimization (PSO) [12, 14], which, in this case, from preliminary analyses, outperformed other algorithms available to the authors, as Taguchi [15, 16], Genetic Algorithms [14], and Gray Wolf and Invasive Weed [8, 17]. PSO was run with a population of 30 individuals over 100 iterations but with a stall control which very often ended the iterations at about 50.

It soon becomes apparent that R_{in} was a conflicting parameter, since preliminary optimization always ended with R_{in} hitting its maximum allowed value, hence it was taken out from the optimization variables, and its value fixed to a desired miniaturization level, so as to reduce the problem complexity. At the same time optimization leads to some insight on the design which suggested to eliminate the third section of the stub and the pertinent chamfer. Indeed, as the numerical results in the next section will show, the best design was attained with this simpler geometry.
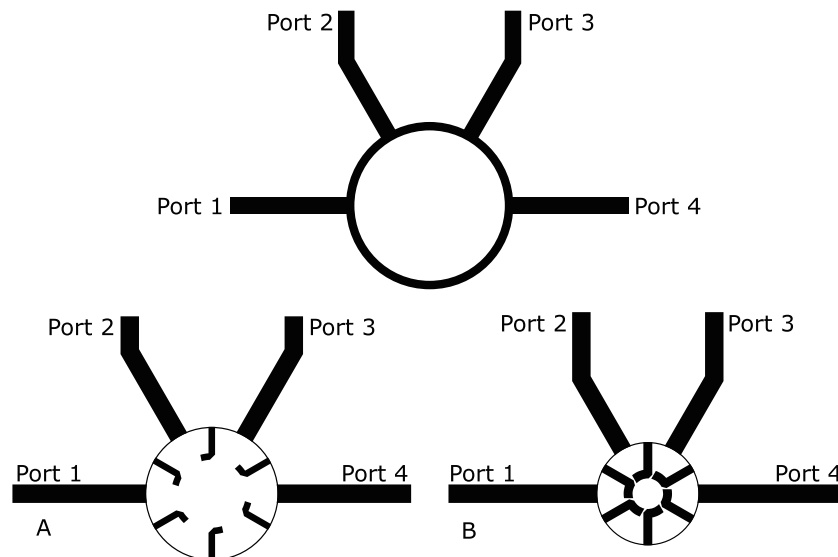
Figure 7. Geometry of the standard rat race, top, and two optimized design, A and B, bottom.

Indeed Design A (Figure 7) was attained on a full set of the 8 optimization variables in Table 1, and it exhibits a quite wide ring and no second bend in the stubs. This, as mentioned before, suggested us to try designs with just 5 optimization variables, dropping l_2 and c_2 completely and fixing R_{in}. This second configuration leads to design B (Figure 7). For both designs, Table 2 reports optimized dimensions. For the B design PSO convergence is also shown in Figure 8.
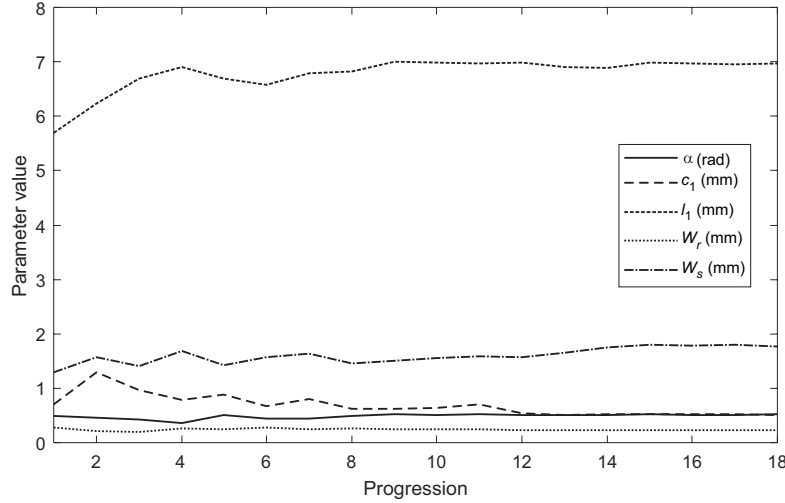
Figure 8. Convergence for the design B, obtained wit PSO with 30 individuals, over 5 parameters (α, c_1, l_1, W_r and W_s). Horizontal axis does not report iteration number (which were 50), but the occurrences of a better cost function value, which does not happen at every iteration.

Table 2. Geometrical parameters for the standard and A and B optimized layouts. Dimensions are in mm, angles in degrees.

Design	R_{in}	W_r	W_s	l_1	c_1	α	Area $(\lambda^2)^{(1)}$
Standard	16.35	1.95	n.a.	n.a.	n.a.	n.a.	0.1998
Design A	12.94	0.233	1.24	5.96	0.681	11.8	0.1035
Design B	$10.00^{(2)}$	0.233	1.76	6.97	0.414	$30^{(3)}$	0.0745

(1) The area is computed as that of the ring: $\pi(R_{in} + W_r)^2$ and normalized to wavelength in the microstrip, taking the average circumference as $2\pi(R_{in} + W_r/2) = 3\lambda/2$.

(2) R_{in} is not among the optimization variables for design B.

(3) α is among the optimization variables for design B and actually hit the optimization upper boundary.

Finally, Table 2 also shows the area of the rat race disk, expressed in terms of squared wavelengths in the microstrip. It is apparent how design A occupies only 52% of the area occupied by a standard rat race, while design B occupies only 37%. Simulations and measurements proving the good electromagnetic behavior are shown in the following section.

4. CHARACTERIZATION

Prototypes of designs A and B have been fabricated on an Isola FR408 substrate ($\epsilon_r = 3.67$, $\tan \delta = 0.012$), Figure 9, and characterized by N5242A PNA X Network Analyzer (10 MHz–25.5 GHz).

Figure 10 shows the amplitude of the scattering parameters measured by feeding ports 1 and 2 (See Figure 7 for port numbering scheme) for design A. The device perfectly symmetric scattering parameters attained by feeding ports 3 and 4 perfectly overlap for simulations and differ only due to
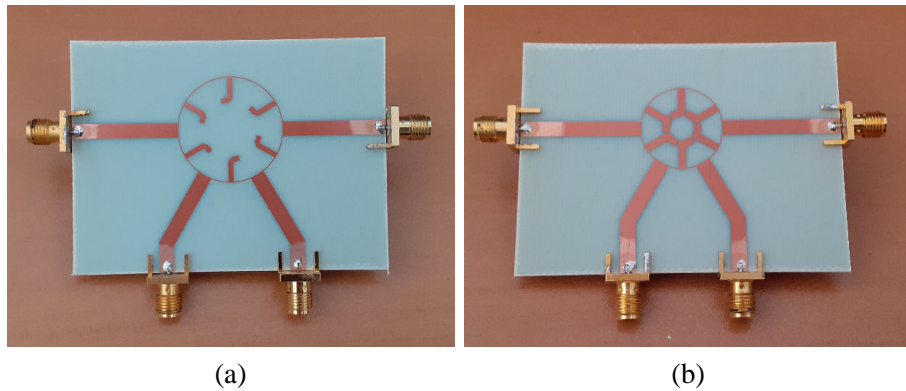
Figure 9. The realized prototypes, respectively for (a) design A, and (b) design B.

Figure 10. Amplitude of the scattering parameters of design A for the case of feeding (a) port 1 and (b) port 2. Measurements are given with solid lines, simulations with dashed lines.

negligible connector effects in measurements. A good agreement between simulations and measurements is apparent, except for S_{11} and, even more noticeably, for S_{22}, possibly due to fabrication issues, and in particular connector welding while the frequency shift between simulations and measurements, in return loss and isolation, is due to the dispersion in the permittivity parameter of the substrate, which is not exactly the nominal one. Phases too, which are given in terms of differential phase shift, have

Figure 11. Error on phase difference for the transmission scattering parameters of design A. S_{12} and S_{32} ought to be in-phase, S_{21} and S_{31} ought to be at $180°$.
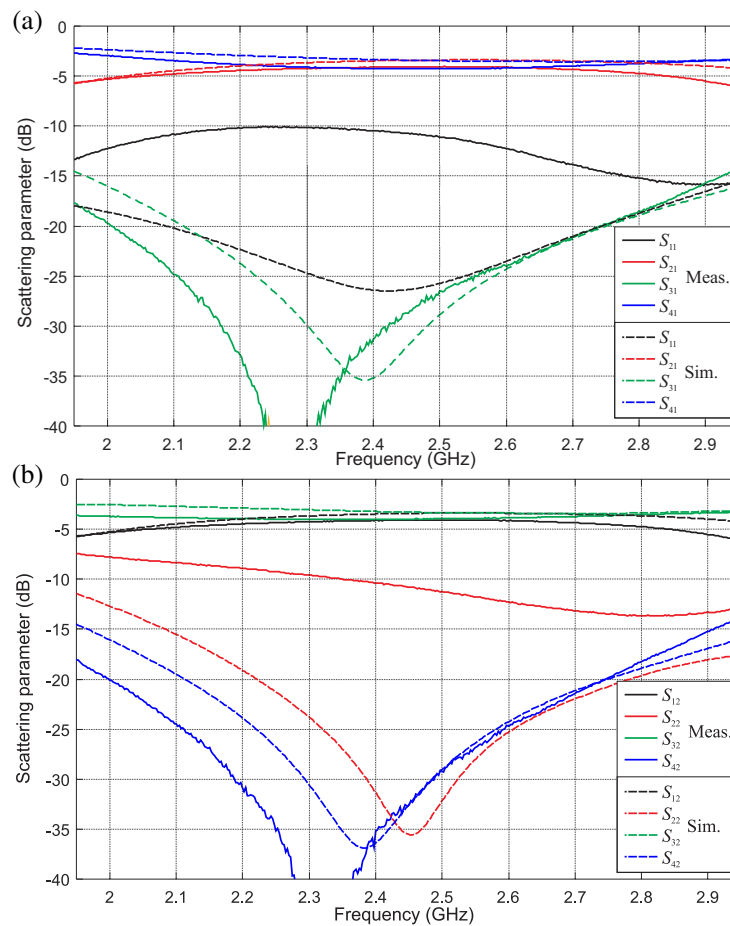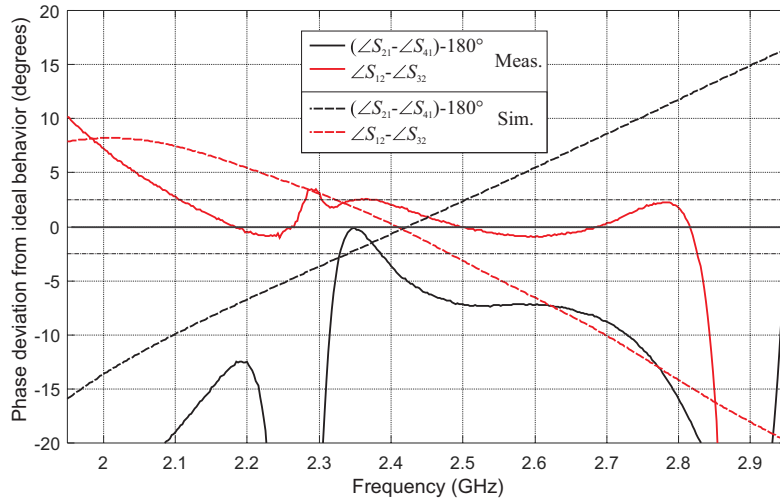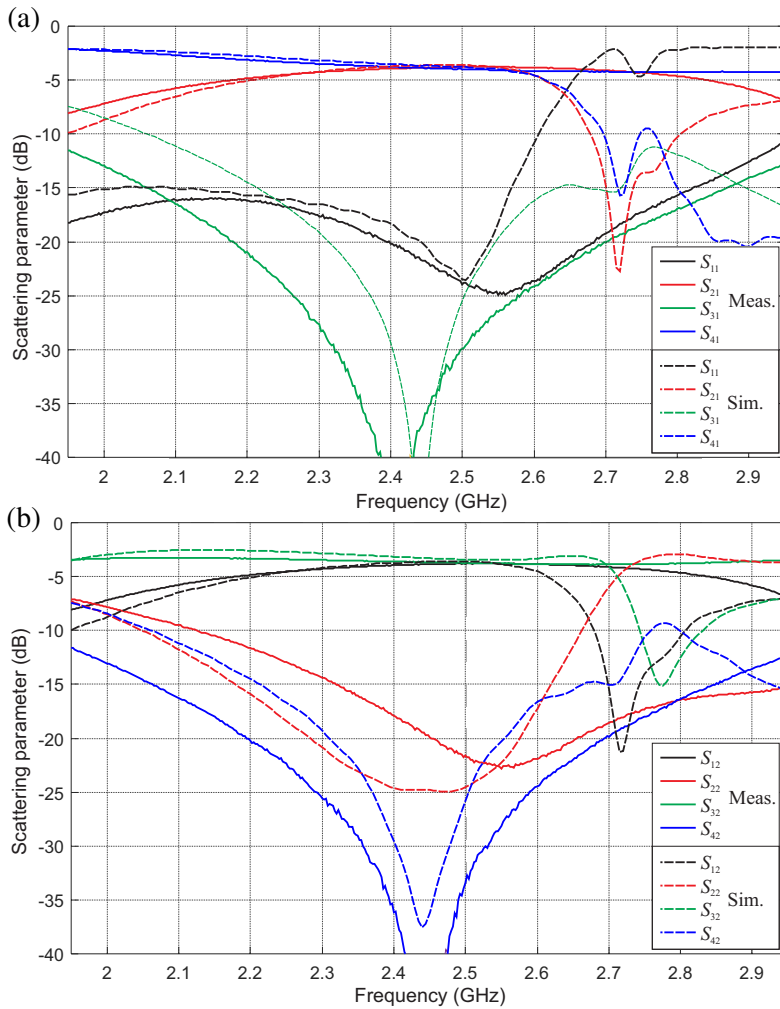

Figure 12. Amplitude of the scattering parameters of design B for the case of feeding (a) port 1 and (b) port 2. Measurements are given with solid lines, simulations with dashed lines.

an overall good behavior, even if phase difference, in measurements, is within $\pm 2.5°$ from nominal on a very narrow band (Fig. 11).

Figure 12 shows the same data for design B. A much better agreement between simulations and measurements is apparent, with a return loss exceeding 15 dB and an isolation even better in measurements than in simulations. Phase too shows a very good behavior.

Table 3. Bandwidths of design B.

	$f_{\min}$ (GHz)	$f_{\max}$ (GHz)	Band (GHz)
S_{11} less than -10 dB	< 1.95	> 2.95	> 1
S_{21} within $[-2, -4]$ dB	2.375	2.677	0.302
S_{31} less than -20 dB	2.175	2.700	0.525
S_{41} within $[-2, -4]$ dB	< 1.95	2.517	> 0.567
S_{22} less than -10 dB	2.117	> 2.95	> 0.833
S_{32} within $[-2, -4]$ dB	< 1.95	> 2.95	> 1
S_{42} less than -20 dB	2.192	2.69	0.498
Amplitude Max ($f_{\min}$) and Min ($f_{\max}$)	2.375	2.517	0.142
$\angle S_{21} - \angle S_{41}$ within $\pm 2.5°$	2.352	2.720	0.368
$\angle S_{12} - \angle S_{32}$ within $180° \pm 2.5°$	2.277	2.615	0.388
Phase Max ($f_{\min}$) and Min ($f_{\max}$)	2.352	2.615	0.263
Overall Max ($f_{\min}$) and Min ($f_{\max}$)	2.375	2.517	0.142

Due to the much better performances of design B, together with its better compactness, Table 3 shows the bandwidth of this latter device only. Transmission coefficients band is defined as the band where amplitude is within -3 dB ± 1 dB. For reflection coefficient, the -10 dB bandwidth is considered, while for isolation the -20 dB bandwidth is considered. For phases, a variation of $\pm 2.5°$ around the nominal value (either zero or $180°$) is considered (Fig. 13).

The overall final bandwidth is 142 MHz, which is about 6% and indeed centered at 2.446 GHz, but it is mainly limited by transmission coefficients, so if a difference larger than 1 dB from nominal -3 dB value is tolerated greater bandwidth is possible. If phase is considered bandwidth is enlarged to 10%, centered on 2.483 GHz.
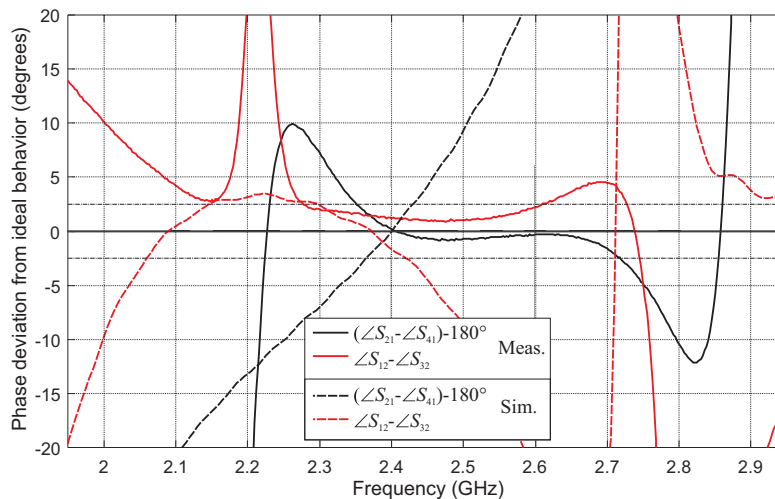
Figure 13. Error on phase difference for the transmission scattering parameters of design B. S_{12} and S_{32} ought to be in-phase, S_{21} and S_{31} ought to be at $180°$.

Table 4. Circuit size comparisons of published compact rat-race couplers compared to this work.

	miniaturization technique	relative circuit size	operative frequency	fabrication process
[18]	microstrip line loaded by open stubs	75%	1.0 GHz	single layer PCB
[19]	reduced length microstrip line	50.7%	0.9 GHz	single layer PCB
[20]	C-SCMRC resonator	45%	2.4 GHz	single layer PCB
[21]	artificial lumped-element LH TL	33%	2.0 GHz	single layer PCB
[22]	periodic open-stub artificial TL	32%	1.8 GHz	single layer PCB
[23]	folded microstrip line	$20 \sim 25\%$	1.5 GHz	single layer PCB
[24]	step-impedance structure	21.5%	2.45 GHz	single layer PCB
[25]	complementary conducting strip TL	13%	5.4 GHz	double layer PCB
[26]	CRLH & periodic open-stub artificial TL	13%	1.8 GHz	single layer PCB
[27]	fractal structure	12.6%	2.4 GHz	single layer PCB
[28]	quasi-lumped artificial TL	9.0%	0.9 GHz	single layer PCB
This paper	artificial shortened TL	37%	2.45 GHz	fully planar PCB

Finally, Table 4 shows a comparison with competing designs available in open literature.

5. CONCLUSIONS

In this letter, two different rat race designs have been proposed. Thanks to the use of bent internal stubs, both devices are miniaturized with respect to the standard one. The area within the circumference of the device, usually "wasted", was used to accommodate six stubs. In particular, design B occupies only 37% of the standard rat race area and shows a bandwidth about 6% at the central frequency.

The reduced dimension of the device proposed allows a tighter integration in complex microwave printed networks, as for example beam forming networks for multibeam antennas [29], with apparent advantages in compactness, light weight, and cost reductions. Performances, in terms of matching, isolation, bandwidth, and losses are comparable to those of conventional rat races.

REFERENCES

1. Collin, R. E., *Foundations for Microwave Engineering*, John Wiley & Sons, 2007.
2. Pozar, D. M., *Microwave Engineering*, John Wiley & Sons, 2011.
3. Fooks, E. H. and R. A. Zakarevicius, *Microwave Engineering Using Microstrip Circuits*, Prentice-Hall, Inc., 1990.
4. Rao, P., *Design of Wide Band Hybrid Coupler*, LAP LAMBERT Academic Publishing, 2013.
5. Maddio, S., G. Pelosi, M. Righini, and S. Selleri, "Balanaced loaded transmission lines applied to hybrid couplers design," *2018 IEEE International Symposium on Antennas and Propagation & USNC/URSI National Radio Science Meeting*, 947–948, IEEE, 2018.
6. Maddio, S., G. Pelosi, M. Righini, and S. Selleri, "A novel hybrid coupler design based on the concept of balanced loaded transmission lines," *2019 IEEE International Symposium on Antennas and Propagation and USNC-URSI Radio Science Meeting*, 743–744, IEEE, 2019.
7. Cidronali, A., S. Maddio, N. Giovannelli, and G. Collodi, "Frequency analysis and multiline implementation of compensated impedance inverter for wideband doherty high-power amplifier design," *IEEE Transactions on Microwave Theory and Techniques*, Vol. 64, No. 5, 1359–1372, 2016.

8. Maddio, S., G. Pelosi, M. Righini, and S. Selleri, "A multi-objective invasive weed optimization for broad band sequential rotation networks," *2018 IEEE International Symposium on Antennas and Propagation & USNC/URSI National Radio Science Meeting*, 955–956, IEEE, 2018.

9. Liu, G.-Q., L.-S. Wu, and W.-Y. Yin, "A compact microstrip rat-race coupler with modified lange and T-shaped arms," *Progress In Electromagnetics Research*, Vol. 115, 509–523, 2011.

10. Liu, H., S.-J. Fang, Z. Wang, and Y. Zhou, "Miniaturization of trans-directional coupled line couplers using series inductors," *Progress In Electromagnetics Research C*, Vol. 46, 171–177, 2014.

11. Bernardi, P., R. Cicchetti, G. Pelosi, A. Reatti, S. Selleri, and M. Tatini, "An equivalent circuit for EMI prediction in printed circuit boards featuring a straight-to-bent microstrip line coupling," *Progress In Electromagnetics Research B*, Vol. 5, 107–118, 2008.

12. Selleri, S., M. Mussetta, P. Pirinoli, R. E. Zich, and L. Matekovits, "Some insight over new variations of the particle swarm optimization method," *IEEE Antennas and Wireless Propagation Letters*, Vol. 5, 235–238, 2006.

13. Tseng, C.-H. and H.-J. Chen, "Compact rat-race coupler using shunt-stub-based artificial transmission lines," *IEEE Microwave and Wireless Components Letters*, Vol. 18, No. 11, 734–736, 2008.

14. Agastra, E., G. Pelosi, S. Selleri, and R. Taddei, "Multiobjective optimization techniques," *Wiley Encyclopedia of Electrical and Electronics Engineering*, 1–29, 2014.

15. Agastra, E., G. Pelosi, S. Selleri, and R. Taddei, "Taguchi's method for multi-objective optimization problems," *International Journal of RF and Microwave Computer-Aided Engineering*, Vol. 23, No. 3, 357–366, 2013.

16. Pelosi, G., S. Selleri, and R. Taddei, "A novel multiobjective Taguchi's optimization technique for multibeam array synthesis," *Microwave and Optical Technology Letters*, Vol. 55, No. 8, 1836–1840, 2013.

17. Maddio, S., G. Pelosi, M. Righini, and S. Selleri, "A comparison between grey wolf and invasive weed optimizations applied to microstrip filters," *2019 IEEE International Symposium on Antennas and Propagation and USNC-URSI Radio Science Meeting*, 1033–1034, IEEE, 2019.

18. Chuang, M.-L., "Miniaturized ring coupler of arbitrary reduced size," *IEEE Microwave and Wireless Components Letters*, Vol. 15, No. 1, 16–18, 2005.

19. Mandal, M. K. and S. Sanyal, "Reduced-length rat-race couplers," *IEEE Transactions on Microwave Theory and Techniques*, Vol. 55, No. 12, 2593–2598, 2007.

20. Gu, J. and X. Sun, "Miniaturization and harmonic suppression rat-race coupler using C-SCMRC resonators with distributive equivalent circuit," *IEEE Microwave and Wireless Components Letters*, Vol. 15, No. 12, 880–882, 2005.

21. Okabe, H., C. Caloz, and T. Itoh, "A compact enhanced-bandwidth hybrid ring using an artificial lumped-element left-handed transmission-line section," *IEEE Transactions on Microwave Theory and Techniques*, Vol. 52, No. 3, 798–804, 2004.

22. Eccleston, K. W. and S. H. Ong, "Compact planar microstripline branch-line and rat-race couplers," *IEEE Transactions on Microwave Theory and Techniques*, Vol. 51, No. 10, 2119–2125, 2003.

23. Settaluri, R. K., G. Sundberg, A. Weisshaar, and V. Tripathi, "Compact folded line rat-race hybrid couplers," *IEEE Microwave and Guided Wave Letters*, Vol. 10, No. 2, 61–63, 2000.

24. Kuo, J.-T., J.-S. Wu, and Y.-C. Chiou, "Miniaturized rat race coupler with suppression of spurious passband," *IEEE Microwave and Wireless Components Letters*, Vol. 17, No. 1, 46–48, 2007.

25. Chen, C.-C. and C.-K. Tzuang, "Synthetic quasi-tem meandered transmission lines for compacted microwave integrated circuits," *IEEE Transactions on Microwave Theory and Techniques*, Vol. 52, No. 6, 1637–1647, 2004.

26. Monti, G. and L. Tarricone, "Reduced-size broadband CRLH-ATL rat-race coupler," *2006 European Microwave Conference*, 125–128, IEEE, 2006.

27. Ghali, H. and T. A. Moselhy, "Miniaturized fractal rat-race, branch-line, and coupled-line hybrids," *IEEE Transactions on Microwave Theory and Techniques*, Vol. 52, No. 11, 2513–2520, 2004.

28. Wang, C.-W., T.-G. Ma, and C.-F. Yang, "A new planar artificial transmission line and its applications to a miniaturized butler matrix," *IEEE Transactions on Microwave Theory and Techniques*, Vol. 55, No. 12, 2792–2801, 2007.

29. Maddio, S., A. Cidronali, M. Passafiume, G. Collodi, and S. Maurri, "Fine-grained azimuthal direction of arrival estimation using received signal strengths," *Electronics Letters*, Vol. 53, No. 10, 687–689, 2017.